Applied Catalysis B: Environmental 245 (2019) 360–366

Contents lists available at ScienceDirect

Applied Catalysis B: Environmental

journal homepage: www.elsevier.com/locate/apcatb

Elucidating the roles of metallic Ni and oxygen vacancies in CO_2 hydrogenation over Ni/CeO_2 using isotope exchange and in situ measurements

Lea R. Winter[a,1], Rui Chen[b,1], Xin Chen[c], Kuan Chang[c], Zongyuan Liu[d], Sanjaya D. Senanayake[d], Amani M. Ebrahim[e], Jingguang G. Chen[a,d,*]

[a] Department of Chemical Engineering, Columbia University, New York, NY, 10027, USA
[b] School of Materials Science and Engineering, Nankai University, Tianjin, 300350, China
[c] Department of Chemical Engineering, Tsinghua University, Beijing, 100084, China
[d] Chemistry Division, Brookhaven National Laboratory, Upton, NY, 11973, USA
[e] Department of Materials Science and Engineering, Stony Brook University, Stony Brook, NY, 11794, USA

ARTICLE INFO

Keywords:
CO_2 hydrogenation
CeO_2 reduction
Metallic Ni
Oxygen exchange
AP-XPS

ABSTRACT

Improvement in processes to convert CO_2 to value-added chemicals requires elucidation of catalytic mechanisms. Previous investigations of CO_2 reduction by hydrogen over CeO_2-supported Ni catalysts suggested that the selectivity to CO and CH_4 was related to the Ni loading. In this work we utilized near ambient pressure X-ray photoelectron spectroscopy to confirm that Ni remained metallic under reaction conditions at different Ni loadings. The presence of partially reduced CeO_2 was detected, suggesting that oxygen from CO_2 did not re-oxidize the CeO_x. Isotope exchange studies were performed using $C^{18}O_2$ in a batch reactor equipped with Fourier transform infrared spectroscopy and mass spectrometry to determine the involvement of surface and lattice oxygen. Our results demonstrate that oxygen exchange with the CeO_2 support occurs beyond the surface layer under CO_2 hydrogenation conditions. Kinetic studies also revealed that the oxygen exchange rate is fast with respect to the CO_2 hydrogenation reaction rate and that the CeO_2 oxygen exchange mechanism is modified by Ni.

1. Introduction

The conversion of CO_2 to fuels and chemicals constitutes a means of managing carbon emissions. This scheme involves chemical conversion of on-site emissions or CO_2 captured directly from the air to close the carbon loop [1,2]. Waste CO_2 that is emitted to the atmosphere promotes deleterious climate change, including ocean acidification [3], extreme weather [4,5], and warming-associated events such as coral bleaching [6] and depletion of polar glaciers [7]. Chemically upgrading CO_2 with H_2 generated using renewable sources represents a pragmatic solution, leading to the formation of three types of molecules: CO, methanol, and hydrocarbons [8]. The reverse water gas shift (RWGS) reaction produces CO, which may be upgraded further to produce methanol and hydrocarbons including alkanes and olefins.

The catalytic pathways that control these processes must be elucidated and improved in order to implement this sustainable chemistry on a large scale. Nanoparticles supported on reducible metal oxides have been employed as dual-functional catalysts: oxide supports provide oxygen vacancies to activate CO_2, and metal active sites dissociate molecular hydrogen. Atomic hydrogen then spills over onto the support or onto interfacial sites to hydrogenate the adsorbed CO_2 [9–12]. Nickel supported on ceria is a non-precious, active catalyst for the reduction of CO_2 by hydrogen [13]. However, studies of Ni supported on CeO_2 have reported poor selectivity to CO at higher Ni loading, and low activity but good CO selectivity at very low Ni loading [14–19]. These trends are summarized in Fig. 1. It had been hypothesized that these trends were related to the different Ni oxidation states, where Ni was oxidized and even incorporated into the ceria lattice at low loading and existed as metallic clusters at higher loading [16–18,20]. Oxidized Ni also implies that CO_2 may adsorb on the Ni particles rather than exclusively on the support [21]. However, we recently reported in situ X-ray absorption near edge structure (XANES) data that revealed Ni to be metallic even for a low loading Ni catalyst (0.5 wt%) that was selective to produce CO [19]. The XANES data represent bulk averaged results,

* Corresponding author at: Department of Chemical Engineering, Columbia University, New York, NY, 10027, USA.
E-mail address: jgchen@columbia.edu (J.G. Chen).
[1] These authors contributed equally.

https://doi.org/10.1016/j.apcatb.2018.12.069
Received 13 September 2018; Received in revised form 16 December 2018; Accepted 27 December 2018
Available online 28 December 2018
0926-3373/

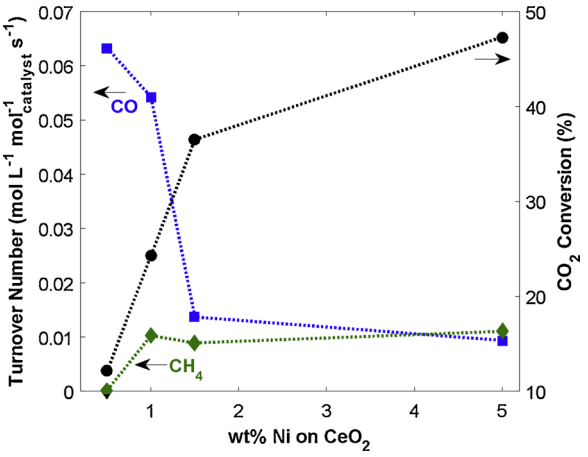

Fig. 1. Summary of activity and selectivity trends for CO_2 reduction by H_2 over Ni/CeO_2 catalysts with different Ni loadings. TON refers to the concentration of the product detected in the gas phase per active site of the given catalyst after a reaction time of 2 h in a batch reactor. The catalyst moles were determined using the catalyst mass and the CO uptake values reported previously for these catalysts [19].

though, rather than direct measurements of the surface, where catalytic reactions actually occur [22].

There has been debate in the literature regarding the correlation of Ni oxidation state and the CO_2 conversion selectivity. Using surface-sensitive in situ AP-XPS, the current study reveals that the oxidation state of Ni remains metallic in both CO-selective and CH_4-selective Ni/CeO_2 catalysts. This result provides direct evidence that the Ni oxidation state at the surface of Ni/CeO_2 catalysts does not explain the selectivity differences. Another novel aspect of the current study is the oxidation state of Ce during CO_2 conversion. CeO_2 is known to undergo partial reduction in the presence of H_2, but CeO_2 is also known to adsorb CO_2 and to facilitate C–O bond scission during catalytic CO_2 reduction by H_2 [23–25]. The combination of these potentially opposing effects, i.e., ceria partial reduction in the presence of H_2 and ceria re-oxidation by oxygen from CO_2 dissociation, has not been resolved previously during the reaction of CO_2 and H_2 over ceria-supported catalysts, to the best of our knowledge. The current study addresses the possibility of reduced ceria being re-oxidized by CO_2 using surface-sensitive AP-XPS measurements in H_2, both with and without CO_2. Since CeO_x does not appear to be re-oxidized by CO_2 under the reaction conditions, isotope exchange experiments have been performed to characterize the dynamic adsorption of oxygen from $C^{18}O_2$ by $Ce^{16}O_x$ during the reaction of CO_2 and H_2. These results provide complementary insights into the interactions between CO_2 and the ceria support during CO_2 hydrogenation over Ni/CeO_2.

2. Experimental methods

2.1. Catalyst preparation

Catalysts were synthesized using incipient wetness impregnation (IWI) over commercial CeO_2 (35-45 m^2/g, Sigma-Aldrich). Precursor salts of $Ni(NO_3)_2{\cdot}6H_2O$ (Alfa Aesar) were dissolved in deionized water and the precursor solution was added drop-wise to the support powder. This mixture was then dried at 363 K for 12 h and calcined at 563 K for 2 h in air. Blank CeO_2 was obtained using the same IWI procedure with deionized water as the precursor solution. The Ni loading amounts were calculated using weight percent, referred to as percent in this paper.

2.2. Catalyst characterization

The surface area of the catalysts was determined by the multi-point BET method using N_2 adsorption isotherms at 77 K (Quantachrome NOVA 2000). Experimental details and results for pulse CO chemisorption, high-resolution transmission electron microscopy, X-ray diffraction, and XANES have been reported elsewhere [19].

Raman spectroscopy was performed on a Bay Spec Raman spectrometer with an optical probe excited at 532 nm (diode pumped solid state green laser) equipped with a CCD detector. Prepared catalysts were stored in sealed vials prior to the measurements.

AP-XPS measurements were carried out at Brookhaven National Laboratory, using a SPECS Phoibos 150-NAP instrument, equipped with a Mg K-α X-ray anode, with an absolute energy resolution of ~0.25 eV for most regions. The catalyst samples were introduced into the analysis chamber under ultra-high vacuum conditions (10^{-9} Torr) followed by pretreatment in 10 mTorr of O_2 at 700 K for 30 min to remove hydrocarbon contaminants. The catalysts were then reduced in 40 mTorr of H_2 at 723 K for 1 h. The samples were then cooled to room temperature in H_2. The reaction was carried out under 50 mTorr with a ratio of 1 CO_2 : 3 H_2. The temperature was held for 30 min each at 300 K, 400 K, 500 K, and 623 K, and scans were taken at each temperature.

2.3. Isotope exchange experiments

A batch reactor equipped with in situ FTIR spectroscopy and mass spectrometry was used to conduct catalytic CO_2 hydrogenation reactions. The experimental apparatus and sample preparation procedure have been reported previously [26]. Between 22–32 mg of catalyst were used, and the exact amount of each catalyst was weighed before loading the samples into the reaction chamber. The catalysts were reduced three times with 30.0 Torr of H_2 for 0.5 h at 723 K, and the reaction chamber was evacuated to below 6×10^{-7} Torr between reductions. Following the reductions, CO_2 and H_2 were introduced into the reaction chamber at a total pressure of 13.0 Torr and a partial pressure ratio of 1 CO_2 : 3 H_2. Concentrations of gas-phase species were monitored using a Thermo Nicolet Nexus 470 spectrometer equipped with a mercury cadmium telluride (MCT-A) detector as described previously [19,25]. The FTIR spectra of gas-phase species were recorded as a function of time at 623 K for 2 h. In order to identify whether the oxygen in the CO product was from the CO_2 reactant or the CeO_2 support, carbon dioxide with ^{18}O isotope ($C^{18}O_2$, Sigma-Aldrich 97 atom% ^{18}O) was reacted with H_2. The time-resolved profiles of the gas-phase species were monitored using their characteristic vibrational modes.

Mass spectrometry measurements were obtained for pulses of the initial concentration of reactants and for the final gas mixture after the reaction. The reaction chamber was connected directly to the mass spectrometer and isolated by a valve. The data were collected using a quadrupole residual gas analyzer (Stanford Research Systems RGA 100). The percentages of the species were compared to known concentrations prepared in the gas handling system; the concentrations obtained from the RGA spectra for CO_2 and CO were in agreement with the as-prepared concentrations to within 5%. The species were monitored at unique m/z values for $C^{18}O_2$ (48), $C^{16}O^{18}O$ (46), $C^{16}O_2$ (44), $C^{18}O$ (30), $C^{16}O$ (28), H_2O (18), CH_4 (15), and H_2 (2), using appropriate sensitivity factors for the cracking patterns of the gases.

3. Results and discussion

3.1. Catalyst redox chemistry under reaction conditions

A comprehensive understanding of the mechanism of CO_2 hydrogenation over supported catalysts requires accurate determination of the oxidation states of the catalytic components under reaction conditions. For the reduction of CO_2 by H_2 over CeO_2-supported Ni catalysts, there are discrepancies in the literature regarding the oxidation state of Ni and how it may control the reaction selectivity summarized in Fig. 1. Recently, results from in situ XANES measurements suggested that Ni remains predominantly metallic during the reaction [19]. However,

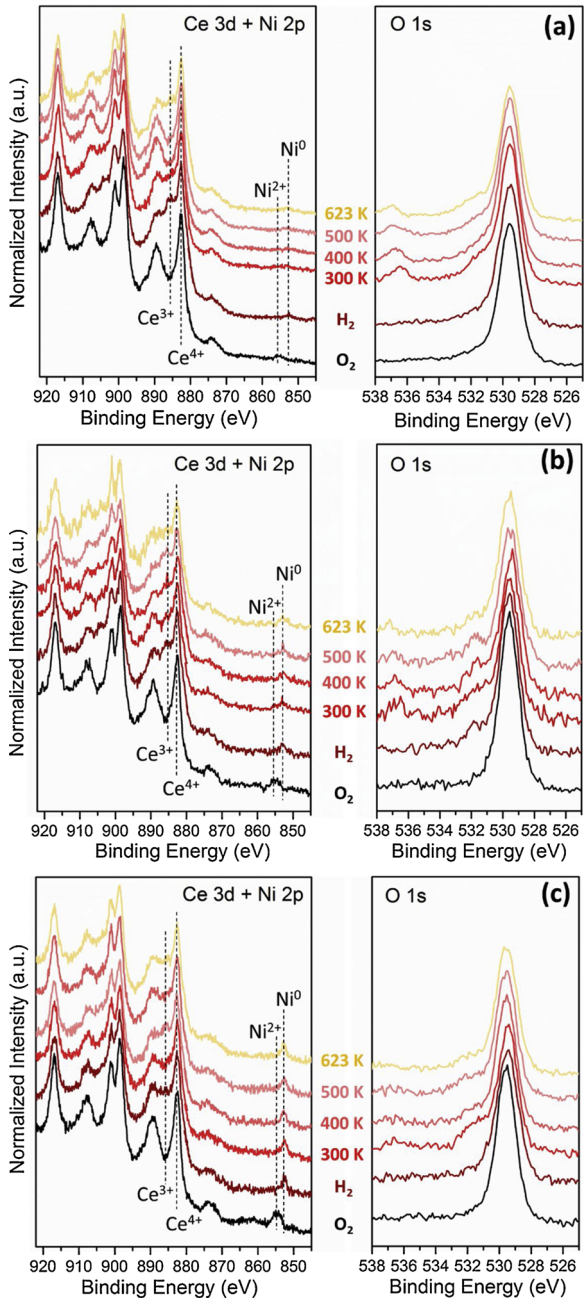

Fig. 2. In situ AP-XPS spectra during H_2 reduction (40 mTorr) and the CO_2 hydrogenation reaction (50 mTorr) over (a) 0.5% Ni/CeO_2, (b) 1.5% Ni/CeO_2, and (c) 5% Ni/CeO_2. Signals from Ce^{4+}, Ce^{3+}, Ni^{2+}, and Ni^0 are indicated.

XANES is a bulk averaging technique and might not adequately reveal the surface properties. In order to investigate the oxidation state of Ni at the surface of the catalyst to explain the CO_2 hydrogenation trends in Fig. 1, AP-XPS was employed for this catalytic system.

The CeO_2-supported catalysts with varied Ni loadings (0.5%, 1.5%, and 5%) were characterized using AP-XPS under reduction and reaction conditions. The results from the Ce 4d, Ni 2p and O1s regions are provided in Fig. 2. For all three catalysts, there was a prominent Ni^{2+} peak under O_2 (10 mTorr) at 723 K, without the appearance of the Ni^0 peak. Under the reduction conditions of 723 K in H_2 (40mTorr), the Ni^{2+} peak disappeared, and a Ni^0 peak formed; the intensity of this peak became stronger with higher Ni loading. Under the reaction conditions of CO_2 and H_2 (50 mTorr), the metallic Ni peak remained at all temperatures, and no Ni^{2+} peak was observed. These results confirm that surface Ni remains metallic under CO_2 hydrogenation reaction conditions; variation in Ni oxidation state with Ni loading cannot account for the trends in reaction selectivity observed for CO_2 hydrogenation over Ni/CeO_2 catalysts.

The AP-XPS results suggest that the CeO_x support plays a central role in oxygen abstraction from CO_2. For all three catalysts, Ce^{4+} was reduced to a mixture of Ce^{3+} and Ce^{4+} under reducing conditions. Upon exposure to CO_2 and H_2, this mixture of Ce oxidation states was maintained for all temperatures, and Ce was not re-oxidized. Together, these results reveal that Ce is not fully oxidized during the reaction, consistent with the hypothesis that partially reduced ceria plays a central role in CO_2 activation.

3.2. Oxygen exchange under reaction conditions

3.2.1. Qualitative exchange trends from in situ FTIR spectroscopy

The involvement of the CeO_x support in the reaction was investigated using $C^{18}O_2$ isotope gas in order to trace the origin of oxygen-containing products, with ^{18}O originating from $C^{18}O_2$ and ^{16}O from the $Ce^{16}O_x$ support.

The inert, irreducible oxide SiO_2 was employed as a control. The FTIR spectra of the gas phase during the reaction of CO_2 + H_2 over 1.5% Ni/SiO_2 are presented in Fig. 3 in the region of the stretching frequencies for $C^{18}O_2$ at 2308 and 2325 cm^{-1} with combination bands at 3510, 3539, 3653 and 3625 cm^{-1}, and for $C^{18}O$ at 2075 and 2118 cm^{-1}. There were no ^{16}O-containing species detected in these spectra, consistent with the conclusion that Ni and NiO alone – in the absence of CeO_2 – are not responsible for CO_2 adsorption and oxygen exchange.

The CO_2 hydrogenation reaction was carried out over CeO_2-supported catalysts with 0%, 0.5%, 1.5%, and 5% Ni loadings. The regions of the IR spectra containing CO_2 and CO signatures are presented for all four catalysts in Fig. 4. Spectra are included for selected time points during the reaction.

The blank ceria catalyst showed no activity toward the CO_2 hydrogenation reaction, as confirmed by the absence of the CO product in the spectra in Fig. 4a. This catalyst did show oxygen exchange activity: at the beginning of the reaction, peaks for the dosed reactant $C^{18}O_2$ were observed at 2308 and 2325 cm^{-1} with the corresponding combination bands in the region between 3510 and 3625 cm^{-1}. Shortly after the initial dose, a third peak rapidly appeared at 2337 cm^{-1} with combination bands at 3583 and 3689 cm^{-1}, indicating the presence of $C^{16}O^{18}O$. A shoulder on the higher wavenumber side of these peaks suggested the presence of a small amount of $C^{16}O_2$ (2357 cm^{-1}), with a small combination band at 3729 cm^{-1}. After 115 min, the $C^{18}O_2$ peak had decreased slightly with a simultaneous increase in the $C^{16}O^{18}O$ peak.

The isotope exchange trends in the CO_2 peaks became more pronounced when the reaction was carried out over 0.5% Ni/CeO_2. The $C^{18}O_2$ peak at 2308 cm^{-1} and its combination bands decreased steadily throughout the reaction (Fig. 4b). The $C^{16}O^{18}O$ peak at 2337 cm^{-1} and the corresponding combination modes increased rapidly, remained fairly constant, and then decreased slightly as this gas species was further consumed in the reaction. This catalyst was active for the CO_2 hydrogenation reaction, producing CO, H_2O, and small amounts of CH_4 [19]. Both $C^{18}O$ (2075 cm^{-1}) and $C^{16}O$ (2158 cm^{-1}) were observed in similar amounts throughout the reaction, with overlapping peaks around 2118 cm^{-1}. Peaks for CH_4 are not shown since this species does not participate directly in oxygen exchange, and H_2O peaks are not shown due to interference from baseline fluctuations.

The activity and the selectivity toward methanation instead of toward the RWGS reaction pathway increase with the Ni loading [19]. Fig. 4c–d show rapid increases in the $C^{16}O^{18}O$ peak over 1.5% and 5% Ni/CeO_2, followed by decreases in both $C^{16}O^{18}O$ and $C^{18}O_2$ peaks. The very broad CO_2 peak for the spectra at 115 min suggested the presence of the $C^{16}O_2$ peak at 2357 cm^{-1}. The poor spectral quality in the combination band region was due to significant overlap with H_2O

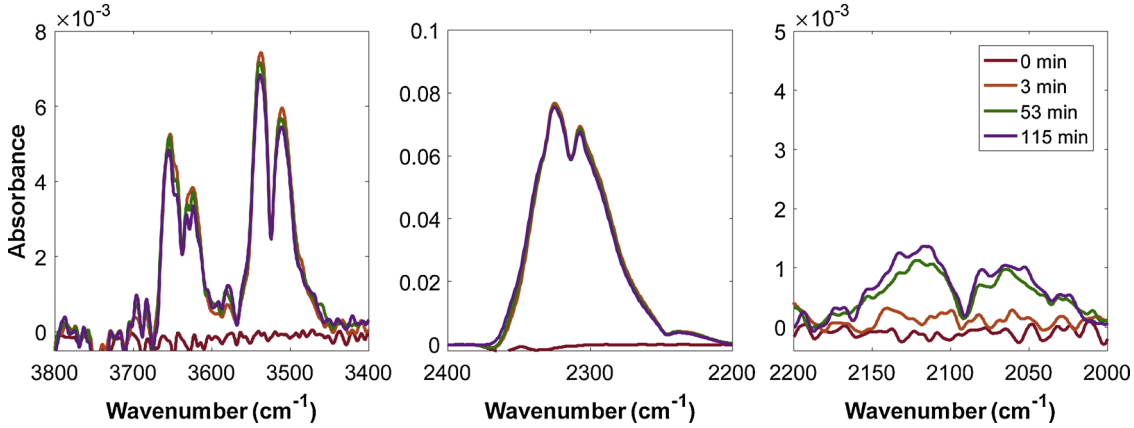

Fig. 3. Time-resolved FTIR spectra of the gas phase during CO_2 hydrogenation over 1.5% Ni/SiO_2, with a total pressure of 13.0 Torr and a partial pressure ratio of 1 CO_2 : 3 H_2.

peaks, where these more active catalysts produced much more H_2O than the 0.5% Ni/CeO_2 and blank CeO_2 catalysts.

3.2.2. Quantitative exchange trends from mass spectrometry

The amount of oxygen donated from the support to the gas phase for varying wt% Ni on CeO_2 was quantified by measuring the concentrations of ^{16}O-containing gases using mass spectrometry. Quantification using the FTIR spectra was insufficient due to the large extent of overlap in the 2000–3000 cm^{-1} region from the stretching modes of the CO_2 and CO isotopes. Although the combination peaks are better resolved, this spectral region was not useful for quantitative analysis due to the overlap with water peaks from the reactions over the more active 1.5% and 5% Ni/CeO_2 catalysts. Therefore, the gas mixture at the end of the reaction was introduced into a mass spectrometer. The total amount of oxygen donated to the gas phase was determined by calibrating the volume of the reaction chamber and by relating the mass spectrometry intensity to the total pressure in the reaction chamber; the moles of gas were then summed as one ^{16}O from $C^{16}O^{18}O$ and from $C^{16}O$, and two from $C^{16}O_2$ to determine the total gas-phase moles of ^{16}O.

In order to calculate the amount of oxygen exchanged with the support, the amount of surface oxygen and bulk oxygen contained in each catalyst sample were calculated as follows:

$$\text{Surface oxygen atoms} = \frac{1\,\text{O atom}}{(5.34\,\text{Å})^2} \times \frac{10^{20}\,\text{Å}^2}{\text{m}^2} \times \frac{1}{N_A} \times S_{BET} \times f_{ceria}\, m_{cat} \quad \text{(E1)}$$

$$\text{Bulk oxygen atoms} = \frac{1\,\text{mol CeO}_2}{172.115\,\text{g}} \times \frac{2\,\text{mol of O atoms}}{1\,\text{mol CeO}_2} \times f_{ceria}\, m_{cat} \quad \text{(E2)}$$

where the CeO_2 lattice parameter is 5.34 Å, N_A is Avogadro's constant, S_{BET} is the BET surface area, f_{ceria} is the percentage of CeO_2 in the sample (excluding Ni), and m_{cat} is the mass of the catalyst. The BET surface area was measured to be 49.1 $m^2\,g^{-1}$ for CeO_2 and 42.4 $m^2\,g^{-1}$ for 5% Ni/CeO_2; these values were linearly interpolated to obtain surface areas for the 0.5% and 1.5% Ni/CeO_2 catalysts.

The calculated amounts of surface and bulk oxygen, as well as the ^{16}O-containing gas-phase products, are reported in Table 1. For all four catalysts, the amount of ^{16}O in the gas phase after reaction exceeded the amount of surface oxygen atoms on CeO_2, derived from BET measurements. For the blank CeO_2 catalyst, 57.6% of the oxygen contained in the bulk sample was exchanged. A similar amount was exchanged for 0.5% Ni/CeO_2. For the catalysts with higher Ni loading, which had higher methanation activity, the percentage of oxygen exchanged was lower by about 10%. The lower exchange amount may be due to the higher methanation activity, where CO_2 is converted to CH_4 rather than to oxygen-containing species. Since methanation produces twice as much water as the RWGS reaction on a CO_2-basis, the water product may contain a higher percentage of exchanged oxygen for the catalysts with higher Ni loading. The isotope content in water was not taken into account due to uncertainties in reliably deconvoluting peaks in the water region. The exclusion of water from the analysis may account for the lower exchanged oxygen amount for the catalysts with higher Ni loading.

To our knowledge, these results provide the first characterization of the extent of CeO_2 oxygen exchange in the presence of H_2. Several previous studies have described CeO_2 oxygen exchange with O_2 and CO_2 gases [27–34]. For example, a $C^{18}O_2$ pulsing and exchange study by Bueno-Lopez et al. reported a distribution of isotope CO_2 species at 623 K of about 40% $C^{18}O_2$, 43% $C^{16}O^{18}O$, and 17% $C^{16}O_2$ (quantities were determined by the authors of the current work through digitization of plotted data reported by Bueno-Lopez et al.) [33]. By comparison, the distribution of the CO_2 isotopes (after 115 min) in the current work over blank CeO_2 was estimated as 39% $C^{18}O_2$, 52% $C^{16}O^{18}O$, and 8.2% $C^{16}O_2$. These quantities were determined using relative intensities of C═O combination bands for each CO_2 isotope, since these bands were well-separated for the reaction over blank CeO_2, and it was assumed that spectroscopic extinction factors among the isotope species were comparable. The total exchange amount over blank CeO_2 was 6690 μmol g^{-1}. By comparison, Martin and Duprez reported 37.7 at nm^{-2} (or 124.3 μmol g^{-1} by our calculations) of oxygen exchanged with CeO_2 using O_2 below 673 K [28]. Based on calculated diffusivity for oxygen in CeO_2-ZrO_2-La_2O_3, Sadovskaya et al. reported a theoretical oxygen exchange amount of 14,945 μmol g^{-1} at 973 K. Based on these comparisons, oxygen exchange may be enhanced by the presence of H_2, and the overall isotope exchange occurred well beyond the surface layer of CeO_2 for all catalysts under the CO_2 and H_2 reaction conditions.

Since the amount of oxygen exchanged was substantial, Raman spectroscopy was employed to provide direct physical measurement of bulk oxygen exchange. The fresh CeO_2 catalyst and the spent CeO_2 catalyst from the $C^{18}O_2$ + H_2 reaction were examined. Fig. 5 shows the Raman active Ce-O F_{2g}/T_{2g} mode representing the symmetric breathing mode of oxygen atoms in the fluorite structure. The spent CeO_2 sample was red shifted (~15 cm^{-1}), confirming the presence of $Ce^{18}O_2$ species resulting from the isotope exchange of $C^{18}O_2$ with the $Ce^{16}O_2$ support.

3.2.3. Oxygen exchange mechanisms and effect of Ni loading

Insights into the mechanism of oxygen exchange with the CeO_2 support and the effect of Ni loading on CeO_2 in the context of the CO_2 hydrogenation reaction may be attained via kinetic analysis of the oxygen-containing species. This analysis was performed using time-resolved in situ FTIR spectroscopic data. The evolution of the isotopes of CO_2 over time for CeO_2 and for 0.5% Ni/CeO_2 are plotted in Fig. 6a–b. The curves are based on the peaks that appear as the C═O combination

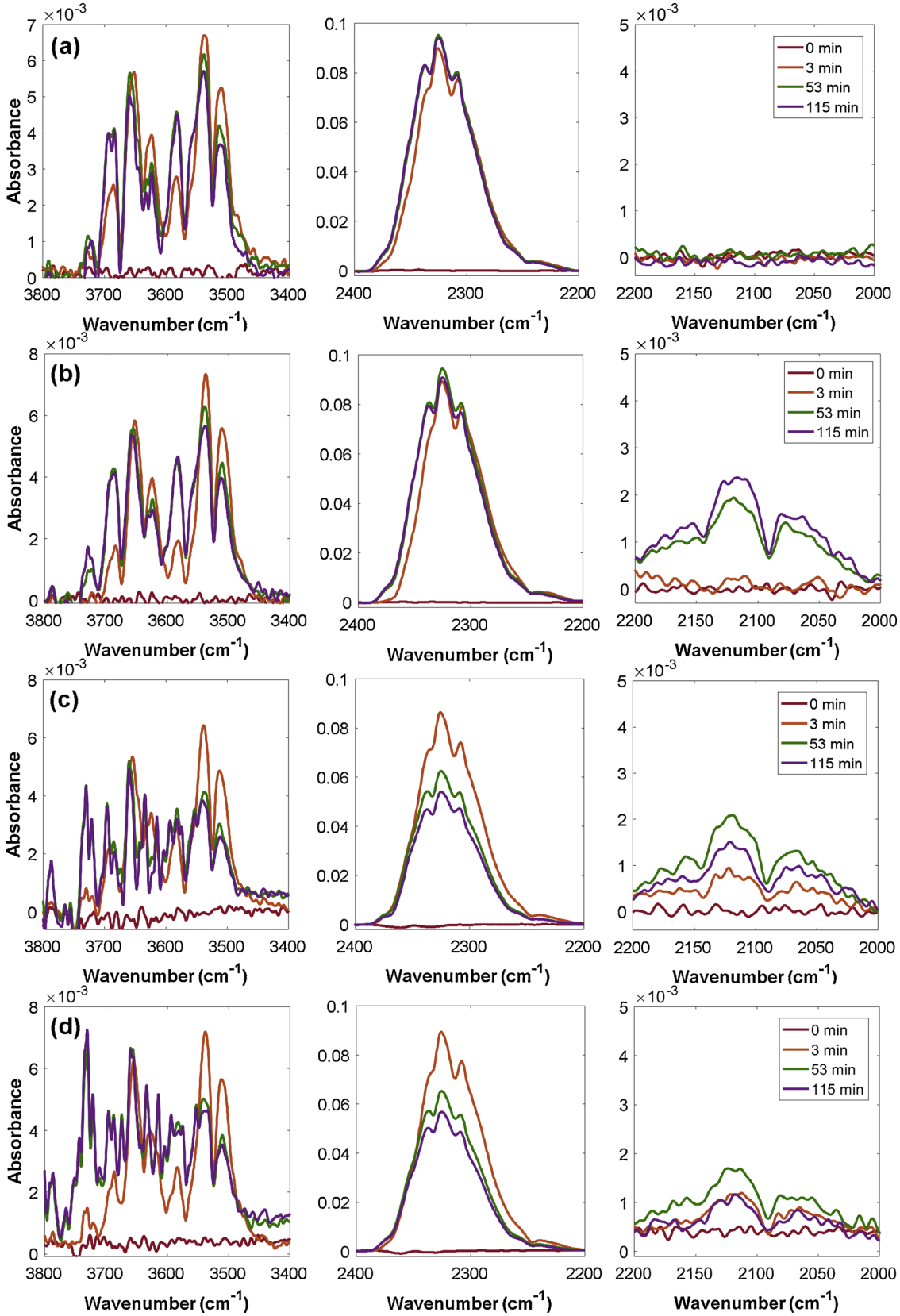

Fig. 4. Time-resolved FTIR spectra of the gas phase during CO_2 hydrogenation over (a) blank CeO_2, (b) 0.5% Ni/CeO_2, (c) 1.5% Ni/CeO_2, and (d) 5% Ni/CeO_2, with a total pressure of 13.0 Torr and a partial pressure ratio of 1 CO_2 : 3 H_2.

bands for each CO_2 isotope ($C^{18}O_2$ at 3510 cm^{-1}, $C^{16}O^{18}O$ at 3583 cm^{-1}, and $C^{16}O_2$ at 3729 cm^{-1}), since these peaks are well-separated with respect to the C═O asymmetric stretching bands around 2300 cm^{-1}. These curves are not available for the 1.5% and 5% Ni/CeO_2 catalysts since the large amount of water formed by the reaction over these catalysts produced substantial interference in this region of

Table 1
Oxygen exchange results based on calculated support oxygen amounts and estimated support-derived oxygen detected in the gas phase using mass spectrometry.

Catalyst	Catalyst mass (mg)	Surface oxygen atoms in sample (μmol)	Total oxygen atoms in sample (μmol)	^{16}O in gas after 115 min (μmol)	% of catalyst oxygen exchanged ($^{16}O_{gas}/^{16}O_{sample}$)	Amount exchanged (μmol $g^{-1}_{CeO_2}$)
CeO_2	25.3	7.23	294	169	57.6%	6690
0.5% Ni/CeO_2	26.1	7.32	301	175	57.9%	6730
1.5% Ni/CeO_2	32.1	8.67	367	175	47.5%	5520
5% Ni/CeO_2	22.5	5.28	248	114	45.7%	5310

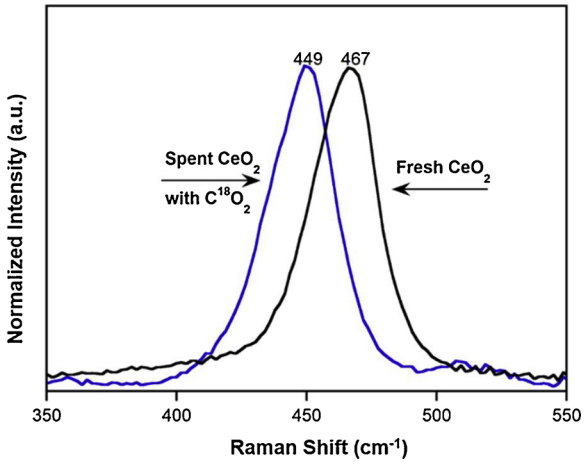

Fig. 5. Raman spectroscopy results for a fresh CeO_2 sample and a sample of CeO_2 used in the reaction of $C^{18}O_2$ + H_2.

the IR spectrum. Therefore, the qualitative exchange kinetics were compared for blank CeO_2 and for 0.5% Ni/CeO_2 only.

The same isotope exchange sequence was observed from the temporal curves in the batch reactor for both blank and 0.5% Ni-doped CeO_2: the reactant $C^{18}O_2$ was consumed rapidly, with the consumption rate decreasing over time; the mixed isotope $C^{16}O^{18}O$ increased and reached a constant equilibrium value after about 40 min; and $C^{16}O_2$ formed more slowly and in smaller amounts, with a decreasing formation rate over time. Oxygen exchange with the support is characterized by three possible mechanisms: 1) homoexchange without participation of support oxygen atoms, 2) simple heteroexchange between one oxygen atom of a gas-phase molecule and one oxygen atom of the oxide support, and 3) multiple heteroexchange between an oxygen-containing gas-phase molecule and at least two oxygen atoms of the support [28,32,35,36]. The results in Fig. 6a–b suggest that oxygen was exchanged by both simple and multiple heteroexchange mechanisms. The exchange appeared to occur in two steps, where one oxygen atom in CO_2 was exchanged rapidly, and exchange of the second oxygen atom occurred subsequently for some of the singly-exchanged $C^{16}O^{18}O$ molecules.

The differences in the curves between the 0.5% Ni/CeO_2 and the blank CeO_2 catalysts provide insight into the role of Ni. A significantly larger amount of $C^{16}O_2$ was formed over Ni/CeO_2 than over blank CeO_2. These results suggest that multiple heteroexchange is promoted by the presence of Ni on CeO_2 with respect to the blank support. Ni promotes H_2 dissociation and should contribute to more facile carbon-oxygen bond breaking. Even though the total oxygen exchange amount was similar for blank CeO_2 and for Ni/CeO_2 (see Table 1), the relative amounts of support-derived, oxygen-containing gas phase products were modified by the addition of Ni.

Fig. 6c shows that CO produced in the reaction over 0.5% Ni/CeO_2 contained both oxygen isotopes. The $C^{16}O$ and $C^{18}O$ production curves closely overlap at low conversion (within the first 20 min). Since the production curves for $C^{16}O$ and $C^{18}O$ followed a similar trend, these results suggest that oxygen exchange was fast with respect to the CO_2 hydrogenation rate.

4. Conclusions

Based on the results discussed above we reveal the complex roles and interplay of Ni and CeO_x during the CO_2 hydrogenation reaction. The following conclusions can be made regarding the role of Ni oxidation state and oxygen isotope exchange with blank and Ni-doped CeO_2 in CO_2 hydrogenation:

1 Ni oxidation state is metallic under CO_2 hydrogenation reaction conditions. Surface-sensitive in situ AP-XPS measurements confirm that Ni remains metallic throughout the reaction for all Ni loadings (0.5%–5% Ni). The Ni oxidation state alone does not explain changes in the product distribution with varied Ni loading on CeO_2.
2 Substantial oxygen exchange occurs between gas-phase species and the ceria support under CO_2 hydrogenation reaction conditions.

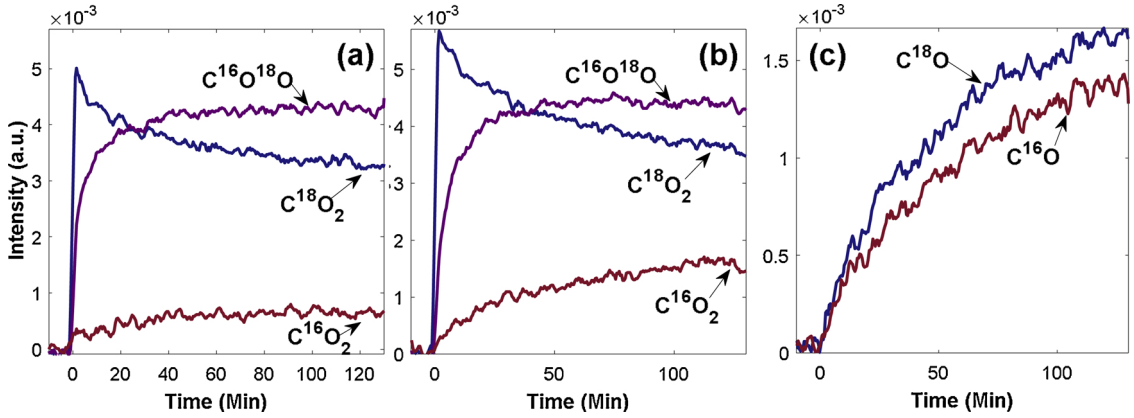

Fig. 6. The evolution of CO_2 isotope peaks over time during the reaction of $C^{18}O_2$ and H_2 over (a) blank CeO_2 and (b) 0.5% Ni/CeO_2. The separable peaks for each isotope were monitored for $C^{18}O_2$ (3510 cm^{-1}), $C^{16}O^{18}O$ (3583 cm^{-1}), and $C^{16}O_2$ (3729 cm^{-1}). (c) The evolution of CO isotope gas concentrations (monitored for $C^{18}O$ at 2070 cm^{-1} and for $C^{16}O$ at 2170 cm^{-1}) over time during the reaction of $C^{18}O_2$ and H_2 over 0.5% Ni/CeO_2.

$C^{18}O_2$ isotope studies using FTIR spectroscopy and mass spectrometry in a batch reactor reveal that oxygen exchange with the support occurs well beyond the surface layer, even in a hydrogen-rich atmosphere. The subsurface oxygen in CeO_x participates in the isotope exchange.

3 The predominant oxygen exchange mechanism over CeO_2 and Ni/CeO_2 catalysts is simple heteroexchange, and multiple heteroexchange also occurs. The addition of metallic Ni to CeO_2 enhances multiple heteroexchange as well as dissociation to CO with exchanged oxygen under CO_2 hydrogenation conditions. Kinetic analysis reveals that the rate of oxygen exchange is fast with respect to the CO_2 hydrogenation reaction rate.

Declarations of interest

None.

Acknowledgements

The work was supported by the US Department of Energy (DE-SC0012704). LRW acknowledges the US National Science Foundation Graduate Research Fellowship Program grant number DGE 16-44869. SDS is partially supported by a U.S. Department of Energy Early Career Award.

Appendix A. Supplementary data

Supplementary material related to this article can be found, in the online version, at doi:https://doi.org/10.1016/j.apcatb.2018.12.069.

References

[1] G. Centi, S. Perathoner, Opportunities and prospects in the chemical recycling of carbon dioxide to fuels, Catal. Today 148 (2009) 191–205, https://doi.org/10.1016/j.cattod.2009.07.075.

[2] S. Perathoner, G. Centi, CO_2 recycling: a key strategy to introduce green energy in the chemical production chain, ChemSusChem. 7 (2014) 1274–1282, https://doi.org/10.1002/cssc.201300926.

[3] S.C. Doney, V.J. Fabry, R.A. Feely, J.A. Kleypas, Ocean acidification: the other CO_2 problem, Annu. Rev. Mar. Sci. 1 (2009) 169–192, https://doi.org/10.1146/annurev.marine.010908.163834.

[4] T.R. Knutson, R.E. Tuleya, Impact of CO_2-induced warming on simulated hurricane intensity and precipitation: sensitivity to the choice of climate model and convective parameterization, J. Clim. 17 (2004) 3477–3495.

[5] J. Hansen, M. Sato, R. Ruedy, K. Lo, D.W. Lea, M. Medina-Elizade, Global temperature change, PNAS 103 (2006) 14288–14293.

[6] T.P. Hughes, J.T. Kerry, M. Álvarez-Noriega, J.G. Álvarez-Romero, K.D. Anderson, A.H. Baird, R.C. Babcock, M. Beger, D.R. Bellwood, R. Berkelmans, T.C. Bridge, I.R. Butler, M. Byrne, N.E. Cantin, S. Comeau, S.R. Connolly, G.S. Cumming, S.J. Dalton, G. Diaz-Pulido, C.M. Eakin, W.F. Figueira, J.P. Gilmour, H.B. Harrison, S.F. Heron, A.S. Hoey, J.P.A. Hobbs, M.O. Hoogenboom, E.V. Kennedy, C.Y. Kuo, J.M. Lough, R.J. Lowe, G. Liu, M.T. McCulloch, H.A. Malcolm, M.J. McWilliam, J.M. Pandolfi, R.J. Pears, M.S. Pratchett, V. Schoepf, T. Simpson, W.J. Skirving, B. Sommer, G. Torda, D.R. Wachenfeld, B.L. Willis, S.K. Wilson, Global warming and recurrent mass bleaching of corals, Nature 543 (2017) 373–377, https://doi.org/10.1038/nature21707.

[7] K. Dow, T.E. Downing, The Atlas of Climate Change: Mapping the World's Greatest Challenge, Third University of California Press, Oakland, CA, 2011.

[8] M.D. Porosoff, B. Yan, J.G. Chen, Catalytic reduction of CO_2 by H_2 for synthesis of CO, methanol and hydrocarbons: challenges and opportunities, Energy Environ. Sci. 9 (2016) 62–73, https://doi.org/10.1039/C5EE02657A.

[9] C.S. Chen, W.H. Cheng, S.S. Lin, Mechanism of CO formation in reverse water–gas shift reaction over Cu/Al_2O_3 catalyst, Catal. Lett. 68 (2000) 45–48.

[10] X. Wang, H. Shi, J.H. Kwak, J. Szanyi, Mechanism of CO_2Hydrogenation on Pd/Al_2O_3 Catalysts: Kinetics and Transient DRIFTS-MS Studies, ACS Catal. 5 (2015) 6337–6349, https://doi.org/10.1021/acscatal.5b01464.

[11] W.C. Conner, J.L. Falconer, Spillover in heterogeneous catalysis, Chem. Rev. 95 (1995) 759–708.

[12] C.S. Chen, W.H. Cheng, S.S. Lin, Study of reverse water gas shift reaction by TPD, TPR and CO_2 hydrogenation over potassium-promoted Cu/SiO_2 catalyst, Appl. Catal. A Gen. 238 (2003) 55–67.

[13] S. Tada, T. Shimizu, H. Kameyama, T. Haneda, R. Kikuchi, Ni/CeO_2 catalysts with high CO_2 methanation activity and high CH_4 selectivity at low temperatures, Int. J. Hydrogen Energy 37 (2012) 5527–5531, https://doi.org/10.1016/j.ijhydene.2011.12.122.

[14] B. Lu, K. Kawamoto, Preparation of the highly loaded and well-dispersed NiO/SBA-15 for methanation of producer gas, RSC Adv. 2 (2012) 6800–6805, https://doi.org/10.1016/j.fuel.2012.09.009.

[15] B. Lu, K. Kawamoto, Preparation of monodispersed NiO particles in SBA-15, and its enhanced selectivity for reverse water gas shift reaction, J. Environ. Chem. Eng. 1 (2013) 300–309, https://doi.org/10.1016/j.jece.2013.05.008.

[16] B. Lu, K. Kawamoto, Preparation of mesoporous CeO_2 and monodispersed NiO particles in CeO_2, and enhanced selectivity of NiO/CeO_2 for reverse water gas shift reaction, Mater. Res. Bull. 53 (2014) 70–78, https://doi.org/10.1016/j.materresbull.2014.01.043.

[17] J. Carrasco, L. Barrio, P. Liu, J.A. Rodriguez, M.V. Ganduglia-Pirovano, Theoretical studies of the adsorption of CO and C on Ni(111) and Ni/CeO_2(111): evidence of a strong metal-support interaction, J. Phys. Chem. C 117 (2013) 8241–8250, https://doi.org/10.1021/jp400430r.

[18] S.D. Senanayake, J. Evans, S. Agnoli, L. Barrio, T.L. Chen, J. Hrbek, J.A. Rodriguez, Water-gas shift and CO methanation reactions over Ni-CeO_2(111) catalysts, Top. Catal. 54 (2011) 34–41, https://doi.org/10.1007/s11244-011-9645-6.

[19] L.R. Winter, E. Gomez, B. Yan, S. Yao, J.G. Chen, Tuning Ni-catalyzed CO_2 hydrogenation selectivity via Ni-ceria support interactions and Ni-Fe bimetallic formation, Appl. Catal. B Environ. 224 (2018) 442–450, https://doi.org/10.1016/j.apcatb.2017.10.036.

[20] N.M. Deraz, Effect of NiO content on structural, surface and catalytic characteristics of nano-crystalline NiO/CeO_2 system, Ceram. Int. 38 (2012) 747–753, https://doi.org/10.1016/j.ceramint.2011.07.068.

[21] X. Du, D. Zhang, L. Shi, R. Gao, J. Zhang, Morphology dependence of catalytic properties of Ni/CeO_2 nanostructures for carbon dioxide reforming of methane, J. Phys. Chem. C 116 (2012) 10009–10016.

[22] J.G. Chen, NEXAFS investigations of transition metal oxides, nitrides, carbides, sulfides and other interstitial compounds, Surf. Sci. Rep. 30 (1997) 1–152, https://doi.org/10.1016/S0167-5729(97)00011-3.

[23] N. Laosiripojana, S. Assabumrungrat, Catalytic dry reforming of methane over high surface area ceria, Appl. Catal. B Environ. 60 (2005) 107–116, https://doi.org/10.1016/j.apcatb.2005.03.001.

[24] T. Staudt, Y. Lykhach, N. Tsud, T. Skála, K.C. Prince, V. Matolín, J. Libuda, Ceria reoxidation by CO_2: A model study, J. Catal. 275 (2010) 181–185, https://doi.org/10.1016/j.jcat.2010.07.032.

[25] M.D. Porosoff, J.G. Chen, Trends in the catalytic reduction of CO_2 by hydrogen over supported monometallic and bimetallic catalysts, J. Catal. 301 (2013) 30–37, https://doi.org/10.1016/j.jcat.2013.01.022.

[26] W.W. Lonergan, D.G. Vlachos, J.G. Chen, Correlating extent of Pt–Ni bond formation with low-temperature hydrogenation of benzene and 1,3-butadiene over supported Pt/Ni bimetallic catalysts, J. Catal. 271 (2010) 239–250, https://doi.org/10.1016/j.jcat.2010.01.019.

[27] T. Jin, T. Okuhara, G.J. Mains, J.M. White, Temperature-programmed desorption of CO and $CO_2$from Pt/CeO_2. An important role for lattice oxygen in CO Oxidation, J. Phys. Chem. 91 (1987) 3310–3315.

[28] D. Martin, D. Duprez, Mobility of surface species on oxides. 1. Isotopic exchange of $^{18}O_2$ with ^{16}O of SiO_2, Al_2O_3, ZrO_2, MgO, CeO_2, and CeO_2-Al_2O_3. Activation by noble metals. correlation with oxide basicity, J. Phys. Chem. 100 (1996) 9429–9438.

[29] C.E. Hori, H. Permana, K.Y.S. Ng, A. Brenner, K. More, K.M. Rahmoeller, D. Belton, Thermal stability of oxygen storage properties in a mixed CeO_2-ZrO_2 system, Appl. Catal. B Environ. 16 (1998) 105–117.

[30] C.E. Hori, A. Brenner, K.Y.S. Ng, K.M. Rahmoeller, D. Belton, Studies of the oxygen release reaction in the platinum-ceria-zirconia system, Catal. Today 50 (1999) 299–308.

[31] F. Dong, A. Suda, T. Tanabe, Y. Nagai, H. Sobukawa, H. Shinjoh, M. Sugiura, C. Descorme, D. Duprez, Dynamic oxygen mobility and a new insight into the role of Zr atoms in three-way catalysts of Pt/CeO_2-ZrO_2, Catal. Today 93–95 (2004) 827–832, https://doi.org/10.1016/j.cattod.2004.06.076.

[32] E.M. Sadovskaya, Y.A. Ivanova, L.G. Pinaeva, G. Grasso, T.G. Kuznetsova, A. Van Veen, V.A. Sadykov, C. Mirodatos, A.V.A. Einstein, F.-V. Cedex, Kinetics of oxygen exchange over CeO_2-ZrO_2 fluorite-based catalysts, J. Phys. Chem. A 111 (2007) 4498–4505.

[33] A. Bueno-Lopez, K. Krishna, M. Makkee, Oxygen exchange mechanism between isotopic CO_2 and Pt/CeO_2, Appl. Catal. A Gen. 342 (2008) 144–149, https://doi.org/10.1016/j.apcata.2008.03.013.

[34] Y. Madier, C. Descorme, a M.Le Govic, D. Duprez, Oxygen mobility in $CeO_2$and $Ce_xZr_{(1-x)}O_2$ compounds: Study by CO transient oxidation and$^{18}O/^{16}O$ isotopic exchange, J. Phys. Chem. B 103 (1999) 10999–11006, https://doi.org/10.1021/jp991270a.

[35] G.K. Boreskov, The catalysis of isotopic exchange in molecular oxygen, in: adv, Catal. Vol. 15 (1964) 285–339.

[36] K.S. Muzykantov, V.V. Popovskii, G.K. Boreskov, Kinetics of isotope exchange in a molecular oxygen-solid oxide system, Kinet. i Katal. 4 (1964).